A characterization of the warm 1999 Arctic winter by observations and modeling: NO_y partitioning and dynamics

M. Stowasser, H. Oelhaf, R. Ruhnke, G. Wetzel, F. Friedl-Vallon, A. Kleinert, W. Kouker, A. Lengel, G. Maucher, H. Nordmeyer, Th. Reddmann, O. Trieschmann, T. v. Clarmann, and H. Fischer

Institut für Meteorologie und Klimaforschung, Forschungszentrum Karlsruhe, Universität Karlsruhe, Karlsruhe, Germany

M. P. Chipperfield

School of the Environment, University of Leeds, UK

Received 15 August 2001; revised 21 November 2001; accepted 2 January 2002; published 5 October 2002.

[1] A characterization of the NO_y partitioning in the warm Arctic winter 1998/1999 is given. Vertical profiles of nocturnal total reactive nitrogen ($NO_y = NO_2 + HNO_3 + ClONO_2 + 2\ N_2O_5 + HO_2NO_2$) were retrieved from infrared limb emission spectra measured by the Michelson Interferometer for Passive Atmospheric Sounding, Balloon-borne version (MIPAS-B) instrument inside a distortion of the winter Arctic vortex from Kiruna (Sweden, 68°N) on 27 January 1999. To estimate the dynamic effects, the mixing ratios of the tracers N_2O and CH_4 were derived to construct a correlation between these two long-lived species and to estimate the effects of mixing on the N_2O-NO_y relationship. The measured data are compared to calculations performed with the three-dimensional chemistry transport models (CTMs) SLIMCAT and KASIMA. The results show that despite the warm winter 1998/1999 without significant occurrence of polar stratospheric clouds, the agreement between both the measurement and the models and among the models themselves is not satisfactory. It appears that in such a dynamically active winter, mixing processes on different scales which are hard to reproduce with coarsely resolved CTMs should be taken into account to explain the differences. Nevertheless, the results indicate that the chemistry which controls the NO_y partitioning is not yet understood well under the studied geophysical situation. Furthermore, chlorine activation appears to be too crudely modeled when winter temperatures are marginal for polar stratospheric cloud formation. *INDEX TERMS:* 0340 Atmospheric Composition and Structure: Middle atmosphere—composition and chemistry; 3360 Meteorology and Atmospheric Dynamics: Remote sensing; 3334 Meteorology and Atmospheric Dynamics: Middle atmosphere dynamics (0341, 0342); 3337 Meteorology and Atmospheric Dynamics: Numerical modeling and data assimilation; *KEYWORDS:* nitrogen partitioning, stratospheric dynamics, mixing processes, modeling, polar ozone, remote sensing

Citation: Stowasser, M., et al., A characterization of the warm 1999 Arctic winter by observations and modeling: NO_y partitioning and dynamics, *J. Geophys. Res.*, *107*(D19), 4376, doi:10.1029/2001JD001217, 2002.

1. Introduction

[2] Nitrogen compounds (NO, NO_2, NO_3, HNO_3, $ClONO_2$, N_2O_5, HO_2NO_2) + ($NO_y = NO + NO_2 + NO_3 + HNO_3 + ClONO_2 + 2\ N_2O_5 + HO_2NO_2$) are involved in chemical processes leading to the destruction of ozone through rapid catalytic cycles. Reservoir species like HNO_3, $ClONO_2$, and N_2O_5 are able to remove reactive species like NO_2 for a certain time from fast chemical reactions. Hence, the partitioning of the individual species within NO_y plays an important role in the chemistry of the winter and spring polar stratospheres.

[3] The main source of NO_y is N_2O transported from the troposphere which reacts with $O(^1D)$ to form NO yielding a compact correlation between N_2O and NO_y. On the other hand, nitric oxide can be photolized and can react with atomic nitrogen causing a loss of NO_y. This loss reaction becomes more important at higher altitudes, thus both competing reactions will lead to a maximum in NO_y in the middle stratosphere [see, e.g., *Brasseur and Solomon*, 1986].

[4] Major contributions to the understanding of stratospheric chemistry have resulted from the investigation of mechanisms which couple the photochemistry of the nitrogen, halogen, and hydrogen families. The coupling which changes the partitioning within the NO_y, Cl_y and HO_x families may occur via gas-phase or heterogeneous reactions [*Hofmann and Solomon*, 1989; *Wennberg et al.*, 1994].

0148-0227/02/2001JD001217$09.00

Though there has been substantial progress in the understanding of these processes, many important details need better explanations before trends in ozone can be understood and predicted [*Solomon et al.*, 1998; *Waibel et al.*, 1999]. Up to now, a quantitative understanding of the partitioning of the nitrogen species has not fully been achieved, although several comparisons have been made between measurements and 1-D, 2-D and 3-D model calculations.

[5] The NO_x/NO_y ratios observed on board the ER-2 in 1991 during the Airborne Arctic Stratospheric Experiment-II (AASE-II) showed differences of up to 50% compared to a photochemical model integrated along back trajectories [*Kawa*, 1993]. A lack of understanding of heterogeneous reactions was suggested to account for the differences. Comparison of the data of the Upper Atmosphere Research Satellite (UARS) for three separate periods between August 1992 and March 1993 with predictions from a constrained version of the Goddard 2-D fixed circulation model showed that the model NO_x/NO_y ratio is systematically lower, especially at higher altitudes [*Morris et al.*, 1997]. Reaction rates and photolysis coefficients in this study were calculated using recommended values from *DeMore et al.* [1994]. *Randeniya et al.* [1999] studied the partitioning of the NO_y family using data obtained from the Halogen Occultation Experiment (HALOE) and a photochemical box model. The use of rate parameters obtained from *DeMore et al.* [1997] in the box model leads to an underestimation of the NO_x/NO_y ratios by 15–35% between 24 and 32 km and 30°–75°N. It was concluded that the gas-phase processes which link NO_x and HNO_3 were inadequately represented in the model. Similar results were found by using data from the Cryogenic Limb Array Etalon Spectrometer (CLAES) and the HALOE instrument compared with box model-calculated monthly averaged NO_x/NO_y ratios and NO, NO_2, and HNO_3 profiles [*Danilin et al.*, 1999].

[6] Since the partitioning of reactive nitrogen is controlled by gas phase and heterogeneous chemistry the atmospheric aerosol loading is important. By 1997 the aerosol loading enhanced by the Pinatubo eruption decreased to a background level [*Thomason et al.*, 1997]. Nevertheless, ER-2 and balloon-borne measurements of the NO_x/NO_y ratios in 1997 show higher values compared to box model simulations [*Gao et al.*, 1999]. The agreement has been improved by including new rate constants for the OH + NO_2 and OH + HNO_3 reactions in the models [*Brown et al.*, 1999a, 1999b; *Dransfield et al.*, 1999; *Portmann et al.*, 1999] instead using kinetic data of *DeMore et al.* [1997]. In Arctic summer and under very low aerosol loading conditions *Osterman et al.* [1999] obtained a promising agreement between observed and modeled NO_x/NO_y ratios.

[7] HNO_3 measurements under a wide range of aerosol surface area densities made with the Smithsonian Astrophysical Observatory Far-Infrared Spectrometer 2 (FIRS-2) covering the period 1989–1997 were given in *Jucks et al.* [1999]. A comparison with a photochemical steady state model using kinetic data of *DeMore et al.* [1997] shows that HNO_3 is significantly overestimated by the model at altitudes above 22 km, with the difference increasing with increasing altitude and decreasing aerosol surface area density. Significantly higher NO_x/HNO_3 ratios were observed by the Atmospheric Trace Molecule Spectroscopy Experiment (ATMOS) in November 1994 in the Antarctic vortex compared to model calculations [*Lary et al.*, 1997]. Results of a photochemical model for the same ATMOS data set using newer kinetic parameters of *DeMore et al.*, [1997] constrained additionally by measurements of the ER-2 aircraft and UARS data yielded a very good agreement for HNO_3 and NO_y at all altitudes inside and outside the Antarctic vortex [*Michelsen et al.*, 1999].

[8] Generally, the NO_x/HNO_3 ratio appears to be fairly well simulated under conditions of high-to-moderate aerosol loading, provided multiphase hydrolysis reactions (N_2O_5 + H_2O, $BrONO_2$ + H_2O) are included. This can be seen in post-Pinatubo NO_y simulations indicating that NO_x (NO/NO_2, NO_2/NO_3) steady state modeling agrees well with observations within experimental uncertainties [*Sen et al.*, 1998]. Similar confidence is associated with constrained modeling of NO_2/N_2O_5 and $NO_2/ClONO_2$ in the lower stratosphere [*Gao et al.*, 1997]. Nevertheless, discrepancies in the order of 20% remain in the lower stratosphere and even larger errors are found in the middle stratosphere [*Gao et al.*, 1999].

[9] Recent 3-D modeling work has shown that in contrast to steady state and constrained models, CTMs do not simulate NO_y distributions very accurately in the stratosphere and that large variations exist among the models. Results of former MIPAS-B flights compared to 3-D model calculations performed with KASIMA (Karlsruhe Simulation model of the Middle Atmosphere) show discrepancies especially in the description of the minor species HO_2NO_2 and N_2O_5 [*Wetzel et al.*, 2002]. Up to now 3-D CTMs generally overestimate denoxification processes inside the polar vortex resulting in low NO_x/NO_y ratios [*Lary et al.*, 1997; *Wetzel et al.*, 1997; *Payan et al.*, 1999].

[10] Together with *Wetzel et al.* [2002], this is the first paper showing the complete nighttime partitioning and budget of NO_y together with N_2O in the Arctic along with results of two 3-D CTMs. Here, we study the warm Arctic winter 1998/99 which was characterized by a disturbed and dynamically active polar vortex. To estimate the dynamic effects the mixing ratios of the tracers N_2O and CH_4 were derived to construct a correlation between these two long-lived species and to estimate the effects of mixing on the N_2O-NO_y relationship. Furthermore we give a characterization of the NO_y budget and compare the results to the output of the two CTMs KASIMA [*Kouker et al.*, 1999] and SLIMCAT [*Chipperfield*, 1999]. In the warm winter 1998/99 without significant occurrence of polar stratospheric clouds together with background aerosol levels, heterogeneous reactions should have played a minor role and we might anticipate good agreement between measurements and model calculations. It is shown that despite this fact the agreement between measurement and model calculations is not satisfactory.

2. Experimental Details

[11] Several types of the Fourier transform spectrometer MIPAS have been constructed for the simultaneous measurement of atmospheric trace gases [*Fischer and Oelhaf*, 1996]. The cryogenic balloon version MIPAS-B was developed to measure limb emission spectra under nighttime or polar winter conditions. The technical details of the instrument are described by *Friedl-Vallon et al.* [1999].

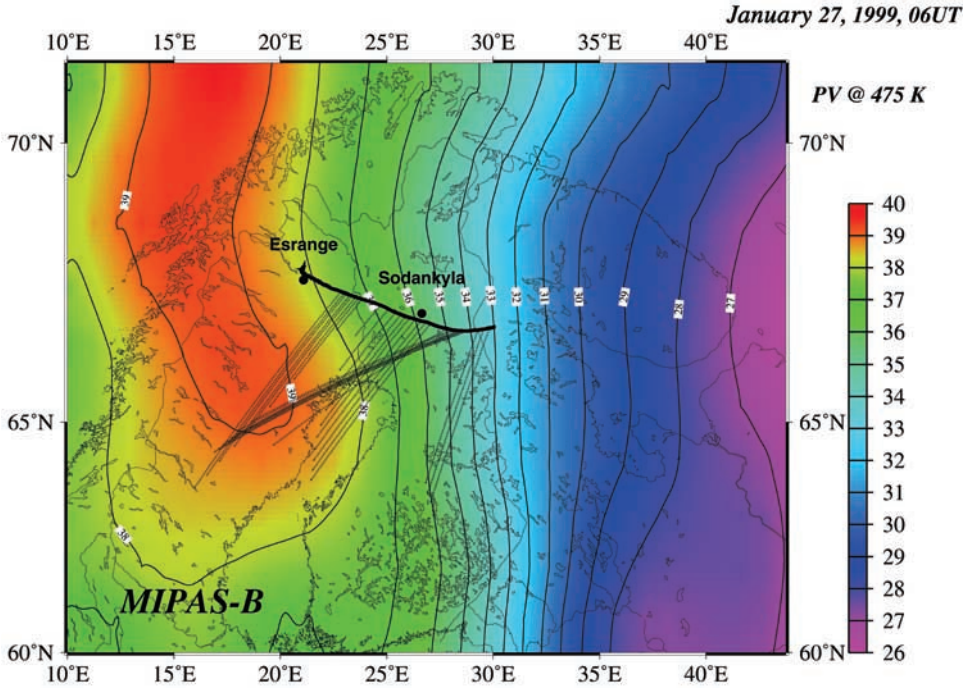

Figure 1. Track of the MIPAS balloon flight starting from Esrange (Kiruna) on 27 January 1999 (thick line). Also plotted are the MIPAS measurement lines of sight (dotted lines, ending at the tangent altitude locations) and the PV contours at 475K (color-coded). The data presented here were obtained during the first limb sequence (left hand side group of lines of sight).

[12] The flight on 27 January 1999 took place from Kiruna (68°N, 21°E) at night inside a distortion of the polar vortex. From a mean float altitude of 32.1 km, eight elevation angles were acquired from −0.71° to −4.65° corresponding to tangent altitudes from 31.4 km down to 10.1 km with a vertical spacing of about 3 km. The azimuth viewing direction was chosen in such a way that the measurement took place inside a tongue of polar vortex air (see Figure 1).

[13] A limb sounding instrument with a spectral resolution of $\Delta\nu \sim 0.07$ cm^{-1} cannot resolve the shapes of vertical profile segments between two tangent altitudes. Therefore the independent parameters to be retrieved are partial slant path column amounts. Between two tangent altitudes the most probable profile form constrained to the retrieved partial column amount was assumed. A high-performance pointing system combined with a CCD star camera system allowed the determination of the tangent altitudes to better than 150 m within a 3 - σ confidence limit [*Maucher*, 1999]. Three spectral channels of the MIPAS-B instrument ranging from 763 to 981 cm^{-1}, 1136 to 1351 cm^{-1}, and 1576 to 1691 cm^{-1} were used to retrieve the trace gas profiles.

3. Data Analysis and Error Estimation

[14] The steps to process the recorded interferograms to calibrated spectra including phase correction and spectral transformation are described by *Trieschmann* [2000]. Special emphasis was placed phase correction in order to achieve a good phase information over the entire range of the channel. Calibration of the spectra was based on recorded "deep space" (+20° elevation angle) and blackbody spectra. Residual atmospheric spectral features in the "deep space" spectra were eliminated to determine the instrumental offset. The gain function of the instrument is derived from the blackbody spectra and the related Planck functions. Calibration and characterization have been described in more detail by *Friedl-Vallon et al.* [1998], *Kleinert and Friedl-Vallon* [1998], *Lengel et al.* [1998], and *Trieschmann and Friedl-Vallon* [1998]. After apodization with the Norton and Beer "strong" function [*Norton and Beer*, 1976], the spectral resolutions ranged from 0.067 to 0.072 cm^{-1}. The noise equivalent spectral radiances (NESRs), after averaging of 5 to 17 spectra recorded at the same elevation angles, range from 1.0×10^{-9} to 4.5×10^{-9} W/(cm^2 sr cm^{-1}), depending on altitude and frequency.

[15] Spectra were analyzed by an onion-peeling retrieval algorithm in combination with a multiparameter non-linear least squares fitting procedure, using the software package Retrieval of Atmospheric Trace gas profiles (RAT) [*von Clarmann*, 1994]. Line-by-line forward calculations were performed with the Fast Atmospheric Signature Code 2 (FASCOD2) algorithm [*Clough et al.*, 1986], which had been modified for inclusion of temperature-dependent cross sections of heavy molecules [*Wetzel et al.*, 1995]. A temperature-pressure first-guess profile was generated with the help of the European Centre for Medium-Range Weather Forecasts (ECMWF) temperatures as well as data from ozone sondes launched shortly before and after the MIPAS flight. The temperature retrieval was performed within selected microwindows of several CO_2 transitions near 810 and 950 cm^{-1}. Atmospheric parameters were fitted in microwindows

Table 1. Location and Temperature Data and Associated Primary Errors (1-σ) for the Flight on 27 January 1999

27 January 1999				Primary Errors	
Pressure, hPa	Altitude, km	Potential Temperature, K	Temperature, K	Temperature, K	Line of Sight, m
6.9	31.4	826.4	199.4	0.8	26
11.7	28.3	715.4	200.7	1.0	29
19.5	25.2	623.9	202.5	0.9	32
32.5	22.2	543.0	203.9	0.9	35
51.7	19.4	479.6	205.8	0.8	37
85.7	16.3	422.3	209.3	1.0	40
148.5	12.8	370.4	214.8	1.0	43
215.2	10.1	333.2	214.8	1.0	46

with relevant spectral contributions of target species using HITRAN96 spectroscopic data [*Rothman et al.*, 1998]. Improved spectroscopic data for HNO_3 transitions in the $\nu_5/2\nu_9$ bands were included (J.-M. Flaud, private communication, 1997). Absorption cross sections for $ClONO_2$ originate from *Birk and Wagner* [2000] and *Oelhaf et al.* [2001], which include temperature-pressure dependencies.

[16] The CO_2 vertical profile was adjusted to its atmospheric abundance in the year 1999, while the initial guess profiles for the other relevant species represent polar vortex standard conditions.

[17] HNO_3 was retrieved within the $\nu_5/2\nu_9$ bands in the spectral interval between 864 and 874 cm^{-1}. Especially at lower altitudes, some interferences caused mainly by CCl_3F and H_2O occur. $ClONO_2$ was analyzed within the Q branch region of the ν_4/ν_3 bands from 779.7 to 780.7 cm^{-1}, while HO_2NO_2 was derived in the Q branch region of the ν_6 band between 802 and 804 cm^{-1}. N_2O_5 was retrieved in the 1220 to 1270 cm^{-1} region of the ν_{12} band in the second MIPAS channel. The N_2O_5 contribution is visible as a broadband pseudo-continuum. Besides N_2O_5, interfering species (e.g. CH_4, N_2O, O_3, H_2O, and COF_2) are fitted simultaneously together with the offset. The source gas N_2O was analyzed around 1160, 1180 and 1260 cm^{-1} ($2\nu_2$ and ν_1 band). NO_2 volume mixing ratios were inferred within the ν_3 band from 1585 to 1615 cm^{-1} which is located in the third channel. Finally, total NO_y was computed by summing up the individual nitrogen components taking into account the number of nitrogen atoms and assuming that the amount of NO is negligible under night time conditions. Methane was retrieved in several microwindows in the spectral interval between 1216 and 1230 cm^{-1}, using the strong lines of the ν_4 band. Main interfering species are O_3 (ν_1 band, centered at 1125 cm^{-1}) and H_2O with some strong lines of the ν_2 band. Spectral contributions of N_2O and N_2O_5 were considered during the forward calculations by their retrieved profiles.

[18] The estimation of random and systematic errors takes into account: (1) spectra random noise as well as covariance effects of the fitted parameters, (2) temperature errors, (3) errors due to an inaccurate knowledge of the line-of-sight, (4) onion-peeling error propagation, and (5) spectroscopic data errors. Spectroscopic errors are estimated on the basis of the HITRAN data base and a study by *Flaud* [1992]. The spectroscopic errors considered were 8% for HNO_3, 5% for $ClONO_2$, N_2O_5, N_2O, and CH_4, 10% for NO_2 and 20% for HO_2NO_2. The primary errors of the temperature and of the line of sight along with the temperature are given in Table 1. Retrieved volume mixing ratios along with the accuracies for the retrieved species are given in Table 2. All errors are given in percent volume mixing ratio (% VMR) and refer to the 1-σ confidence limit. The influence of an incorrect profile shape above the highest tangent altitude was estimated by means of test retrievals assuming an error of 20% in the vertical gradient of the mixing ratio. The total errors of NO_y and of the individual ratios were calculated according to the Gaussian error propagation. A detailed description of the data analysis and the error estimation is given by *von Clarmann et al.* [1997] and *Wetzel et al.* [1997].

4. Model Calculation

[19] Three-dimensional model calculations were performed with the chemistry transport models (CTM) SLIMCAT and KASIMA. KASIMA combines a diagnostic model up to the upper limit (10 hPa) of the ECMWF meteorological analyses with a mechanistic model of the middle atmosphere to account for a more realistic diabatic circulation [*Kouker et al.*, 1999; *Reddmann et al.*, 2001]. The model extends vertically between 10 and 120 km pressure altitude. The SLIMCAT model makes use of UKMO analyses (up to 0.4 hPa) and calculates the transport of the trace species on isentropic levels in contrast to KASIMA which uses pressure levels as vertical coordinate. SLIMCAT uses diagnosed heating rates for the description of the vertical transport. The vertical velocity in the KASIMA model is calculated from the divergence of the horizontal wind fields which are taken from ECMWF analyses. The KASIMA model has a horizontal resolution of 2.8° × 2.8° using 6-hourly wind fields while the SLIMCAT experiment used here has a resolution of 3.75° × 3.75° using 24-hourly wind fields. The reaction rate constants are calculated in both models using the JPL 1997

Table 2. Results From MIPAS-B With Associated Total 1-σ Errors on 27 January 1999[a]

Pressure, hPa	HNO_3, ppbv	$ClONO_2$, ppbv	N_2O_5, ppbv	HO_2NO_2, pptv	NO_2, ppbv	NO_y, ppbv	N_2O, ppbv	CH_4, ppmv
6.9	2.3 ± 14%	1.04 ± 12%	1.71 ± 18%	27 ± 44%	3.4 ± 21%	10.1 ± 10%	12.1 ± 15%	0.41 ± 10%
11.7	7.1 ± 8%	1.26 ± 6%	1.97 ± 13%	62 ± 26%	1.4 ± 26%	13.7 ± 6%	21.2 ± 11%	0.43 ± 10%
19.5	10.3 ± 8%	1.22 ± 6%	0.49 ± 12%	28 ± 28%	0.1 ± 32%	12.6 ± 7%	55.7 ± 11%	0.71 ± 10%
32.5	10.6 ± 8%	1.16 ± 6%	0.08 ± 12%	27 ± 30%	–	11.9 ± 7%	86.5 ± 10%	0.83 ± 11%
51.7	9.9 ± 9%	1.23 ± 7%	0.05 ± 44%	8 ± 36%	–	11.3 ± 8%	98.1 ± 10%	0.87 ± 10%
85.7	5.4 ± 9%	0.69 ± 8%	–	–	–	6.1 ± 8%	210.7 ± 11%	1.34 ± 11%
148.5	1.9 ± 10%	0.14 ± 9%	–	–	–	2.0 ± 9%	274.1 ± 12%	1.56 ± 11%
215.2	0.9 ± 10%	0.03 ± 19%	–	–	–	1.0 ± 10%	299.0 ± 12%	1.68 ± 12%

[a] Abbreviations are as follows: ppbv, parts per billion by volume; pptv, parts per trillion by volume. Dashes indicate no data available.

recommended data with the updates of JPL 2000 [*DeMore et al.*, 1997; *Sander et al.*, 2000]. The seasonal model runs of KASIMA were initialized in the early winter of the corresponding year whereas the results of SLIMCAT had been obtained from a multi-annual run initialized in October 1991. The SLIMCAT run which is used in this comparison uses H_2SO_4 fields from a 2-D model [*Chipperfield*, 1999], while KASIMA uses SAGE II data [*Thomason et al.*, 1997]. The SAGE II data used in KASIMA are more realistic than the 2-D model output used in SLIMCAT, because this 2-D model [*Bekki and Pyle*, 1994] does not reproduce the post-Pinatubo decay beyond 1995 and the model does not produce sufficient descent at high latitudes. For both CTMs the results of the model calculations were calculated for the mean tangent height location and mean time of the MIPAS measurements.

5. Results and Discussion

5.1. Meteorological Situation

[20] The winter 1998/99 was a dynamically active winter with a disturbed, weak vortex [*Manney et al.*, 1999]. The measurement took place in a relatively cold period when the vortex was re-established after a strong warming event in December which had continued through the first 10 days of January. Temperature conditions below the threshold for PSC formation were only present during a small time period between the end of November and mid December. Hence temperatures were not cold enough to form polar stratospheric clouds (PSCs) type 1 (nitric acid trihydrate, NAT) or even type 2 (ice clouds) over extended time periods but often remained close to the NAT temperature threshold. To interpret the observed data, we used maps of Ertel's potential vorticity (EPV) on isentropic surfaces using the ECMWF data. To distinguish whether the measurement took place inside polar vortex air, EPV values of the vortex edge were calculated using the definition of the steepest gradient [*Nash et al.*, 1996]. From this point of view the vortex is more compact in the upper levels, while at lower altitudes the vortex becomes more and more patchy. The EPV values for the polar vortex edge are given in Table 3 and are compared to values of the cold winter 1996/97 as given in *Kondo et al.* [1999]. The comparatively low values imply a weak polar vortex at all altitude levels.

[21] Although the distribution of EPV on isentropic surfaces indicates a more pronounced vortex at higher altitudes, the MIPAS profiles of the two tracers CH_4 and N_2O above 20 km ($\sim$50 hPa) indicate air masses of the vortex edge or strong mixing effects between midlatitude and vortex air masses, while below 50 hPa the comparatively low CH_4 and N_2O values suggest vortex air and a strong subsidence (see Figure 2). The observed structure is seen both in the MIPAS CH_4 (not shown) and in the N_2O profile. The SLIMCAT output of N_2O suggests a stronger subsidence over the entire altitude range compared to the measurement. In contrast KASIMA models significantly larger N_2O values. For comparison a MIPAS N_2O profile measured on 11 February 1995 [*Oelhaf et al.*, 1996], well inside the polar vortex, is also shown revealing much lower volume mixing ratios above 50 hPa. The N_2O profiles are compared to an in-situ profile inside the polar vortex which was obtained one week later from the same location.

Table 3. EPV Values of the Vortex Edge Using the Definition of the Steepest Gradient of PV Compared to Values in February 1997[a]

	January 1999		February 1997
Level, K	Tangent Altitude, PVU	Vortex Edge, PVU	Vortex Edge, PVU
675	202	169	200
625	137	108	–
550	86	63	90
475	39	29	42
435	25	19	–
400	14	13	16

[a] From [*Kondo et al.*, 1999]. Also given are the EPV values at the tangent altitudes. 1 PVU = 10^{-6} km^2 kg^{-1} s^{-1}.

Though there is more structure in the in situ profile the two-pieced profile shape is also seen in this measurement [*Müller et al.*, 2000].

[22] To investigate the observed structures, an analysis of backward trajectories of the air parcels measured on 27 January 1999 was made using the PV thresholds given in Table 3 to distinguish between inside and outside vortex air. The weakness of the vortex as compared to 1997 is evident. The trajectory analysis shows, that for all isentropic levels, the air masses had remained inside the vortex for the last 10 days prior to the observation. For the lowest altitude levels (350K and 380K) the PV values are close to the threshold, above that altitude they are always well above the thresholds. Hence the mixing events producing the signal of large tracer values above 20 km must have occurred earlier in the winter, most likely in the time of the strong minor warming at the end of December.

5.2. Tracer Correlations

[23] In this section we focus on the NO_y-N_2O relationship and the correlation of the two long-lived trace gases N_2O and CH_4. The correlation between the two long-lived tracers N_2O and methane is shown in Figure 3. The solid line represents a mean midlatitude correlation derived from ATMOS data [*Michelsen et al.*, 1998]. The symbols are the results derived from MIPAS observations made inside the Arctic vortex in January 1999 and at midlatitudes in April 1999. A compact linear correlation is found for the winter flight. The results of the April flight fit the midlatitude reference correlation very well. Deviations from this correlation are obvious in the altitude region of a filament at 14.1 hPa corresponding to N_2O values of about 40 ppbv.

[24] The NO_y values are plotted versus the N_2O values in Figure 4. The solid line marks a mean midlatitude correlation derived from ATMOS data [*Michelsen et al.*, 1998]. For comparison an ATMOS correlation based on measurements outside the polar vortices is given [*Sugita et al.*, 1998]. The symbols indicate the results derived from MIPAS observations made inside the Arctic vortex in January 1999 and at midlatitudes in April 1999. For the winter measurement below 19 km (above $\sim$100 ppbv N_2O) the observed NO_y mixing ratios agree very well with those calculated using the ATMOS midlatitude NO_y-N_2O correlation. Above 19 km the NO_y values are up to 2.5 ppbv lower than the reference correlation. This deficit cannot be attributed to denitrification because temperatures were not cold enough to form polar stratospheric clouds type 1 or even type 2 over a sufficiently long time period. The

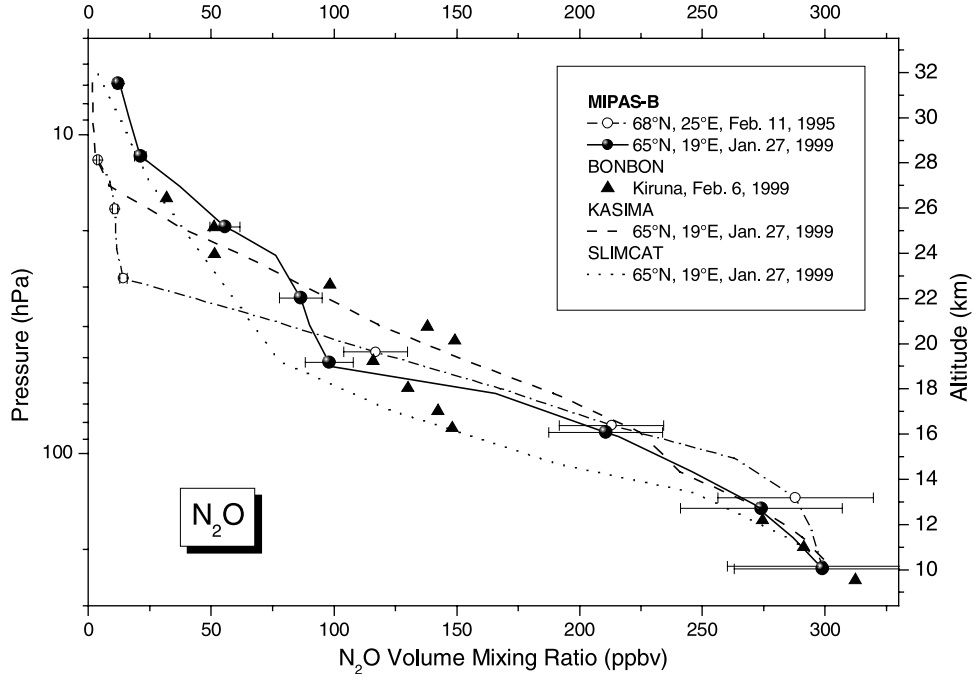

Figure 2. N_2O volume mixing ratios measured by MIPAS-B on 27 January 1999 (solid line with symbols) and modeled by KASIMA (dashed line) and SLIMCAT (dotted line). An in situ observation (BONBON) [*Müller et al.*, 2000] 9 days after the MIPAS flight shows a similar characteristic of the air masses. For comparison a MIPAS N_2O profile measured well inside the polar vortex on February 11, 1995 is shown, too.

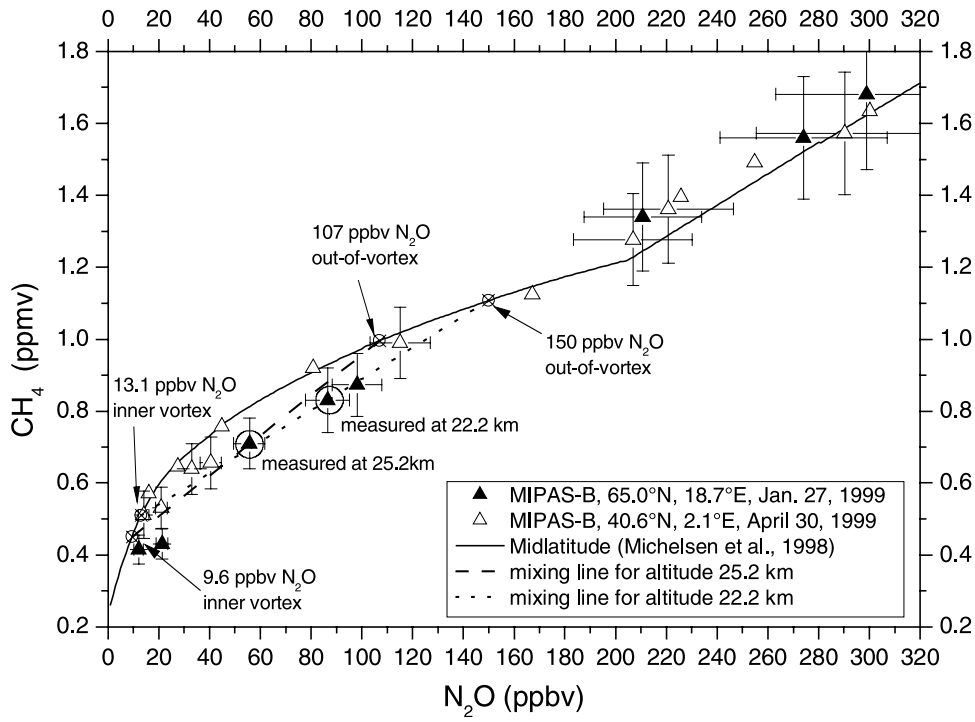

Figure 3. CH_4-N_2O correlation measured by MIPAS-B on Jan. 27, 1999 and April 30, 1999. Two mixing lines for the data points measured at 22.2 and 25.2 km are given. The points where the mixing lines intersect the extra-vortex reference correlation (marked with circles with cross) denote the air masses that have mixed within one single event to produce the properties at the two marked data points. The extra-vortex reference correlation [*Michelsen et al.*, 1998] is in good agreement with the data of the April flight.

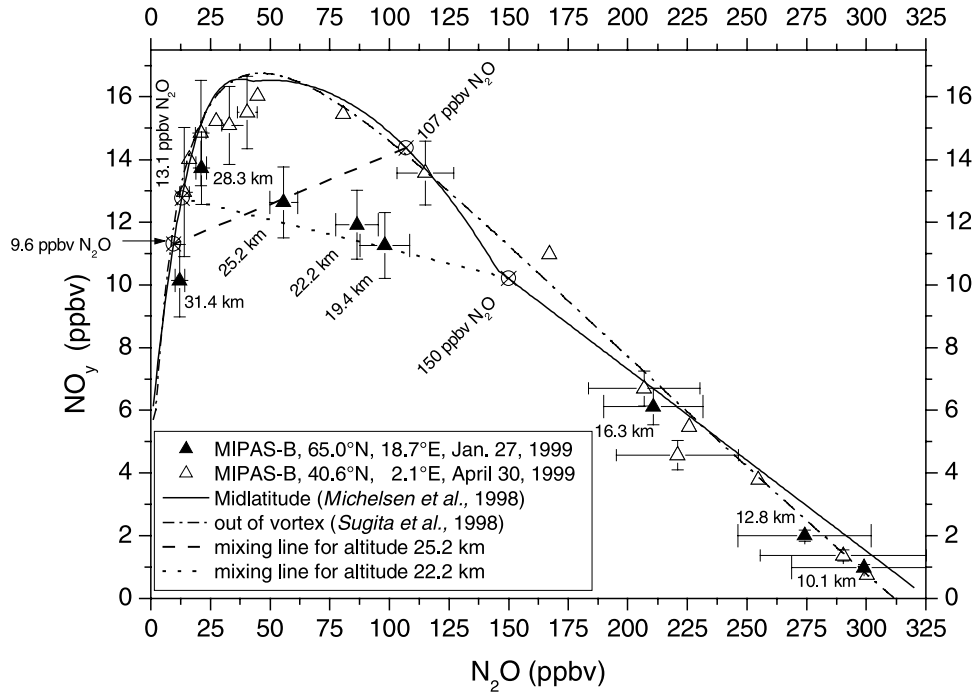

Figure 4. N_2O-NO_y correlation as measured by MIPAS-B on 27 January 1999 and 30 April 1999. Altitude annotations refer to the closest data points of the polar vortex measurement. The two anomalous points at 22.2 and 25.2 km could be explained by diabatic descent and quasi-horizontal mixing of vortex and extra-vortex air. The deduced mixing lines constructed with the help of the CH_4/N_2O data are in good agreement with the measurement. The points where the mixing lines (valid for 22.2 km and 25.2 km altitude) intersect the extra-vortex reference correlation (marked with circles with cross) denote the air masses that have mixed within one single event. The two reference correlations are derived from ATMOS measurements [*Michelsen et al.*, 1998; *Sugita et al.*, 1998].

deviation is attributed to subsidence and mixing processes of vortex air masses with extra-vortex air. The correlation of the two source gases N_2O and CH_4 (not affected by denitrification) helps to estimate the amount of quasi horizontal mixing of two air masses along isentropic surfaces [*Waugh et al.*, 1997; *Michelsen et al.*, 1998; *Rex et al.*, 1999]. If a single mixing event across the vortex edge occurred, the air masses at the measured point at 22.2 km (see Figure 3) should have mixed with air outside the vortex at the same (potential temperature) altitude. This out-of-vortex N_2O value we chose from a standard out-of-vortex profile published by *Michelsen et al.* [1998] yielding the first end member on the standard midlatitude correlation in Figure 3 (circle with cross at 150 ppv N_2O). The straight dashed line through this end member and the measured data point intersects the midlatitude correlation at the second inner vortex end member (circle with cross at 13.1 ppbv N_2O) to create the mixing line. This mixing line can be transferred into the N_2O - NO_y space in Figure 4 with the end members at 150 ppbv N_2O and 13.1 ppbv N_2O on the ATMOS midlatitude correlation. The measured data point at 22 km in Figure 4 lies on this mixing line within the error bars. Therefore the deviation from the ATMOS midlatitude correlation can be explained by the combined process of diabatic descended air and quasi horizontal mixing across the vortex edge. This kind of approach could be interpreted as an 'upper limit' of possible mixing assuming a single mixing event which in reality might have taken place in several mixing events or even continuously [*Plumb et al.*, 2000]. Equal to the scheme described above, the mixing line for the data point at 25.2 km was transferred to the N_2O-NO_y space.

[25] The open symbols illustrate the situation in spring 1999 at midlatitudes. At this time, the MIPAS measurement very closely follows the ATMOS N_2O-NO_y Northern Hemisphere correlation (within the 1-σ error confidence limit). The slight deviation from the correlation between 29 and 33 km (corresponding to 25 to 45 ppbv N_2O) is a hint that the undisturbed midlatitude conditions are not yet re-established at this time. Actually, at this altitude level a remnant filament of polar vortex air is also seen in the midlatitude N_2O profile (not shown here).

5.3. NO_y Partioning: A Comparison With 3-D CTMs

[26] After recording data sets of the partitioning of NO_y in the cold winters 1994/95 and 1996/97 [see, e.g., *Oelhaf et al.*, 1996, 2000; *Wetzel et al.*, 1997, 2002] inside a very strong vortex, we are now able to investigate the NO_y budget in an unusually warm winter with a disturbed but re-established vortex. The complete partitioning and budget of NO_y, measured on 27 January 1999 compared to model calculations performed with the 3-D CTMs SLIMCAT and KASIMA is depicted in Figure 5.

[27] The HNO_3 profile shows a distinct and broad maximum up to 11.8 ppbv around 22.2 km ($\sim$33 hPa). This is fairly consistent with the model calculations. The

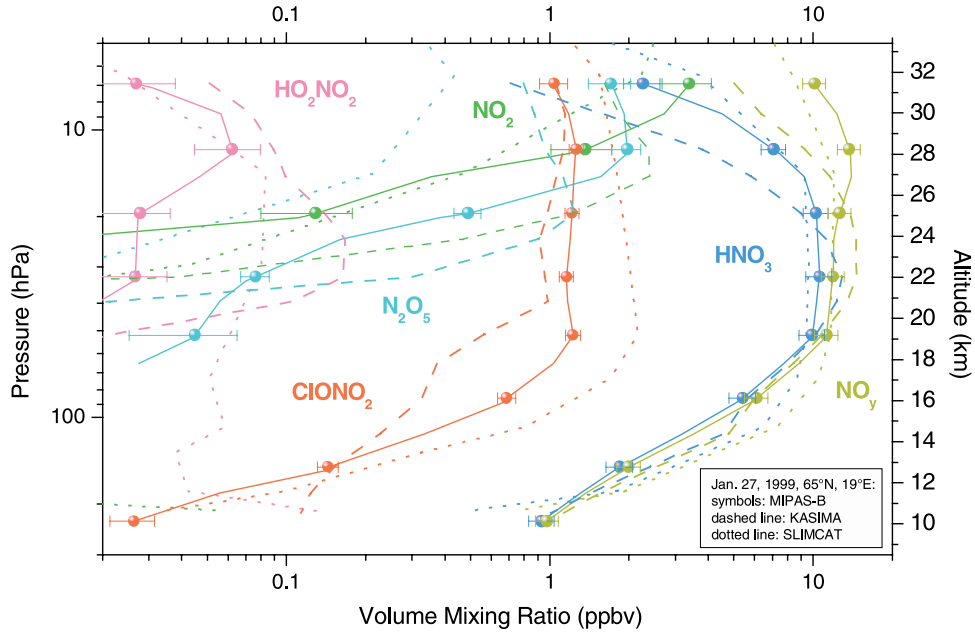

Figure 5. NO_y partitioning as measured on 27 January 1999 (solid lines with symbols) compared to model calculations performed with SLIMCAT (dotted lines) and KASIMA (dashed lines).

SLIMCAT model results reveal an even broader maximum and above 28 km this model overestimates the amount of HNO_3. In contrast the KASIMA model shows an underestimation of HNO_3 in this altitude region. Below this altitude there is a quite good agreement between the measurement and the model outputs. A reasonable agreement had also been seen between the MIPAS profile and the results of the ASUR instrument obtained on the FALCON aircraft that was coordinated with the MIPAS-B flight [*von König et al.*, 2002]. The large mixing ratios of HNO_3 result from strong denoxification processes (conversion of NO_x to HNO_3 mainly via N_2O_5) during the polar winter.

[28] The broad maximum of the $ClONO_2$ profile between 19 and 28 km could be explained by a combination of two effects: (1) The upper part of the maximum is caused by the midlatitude character of the air masses which is also seen in the tracer profiles. (2) the lower part of the maximum results from the recombination of previously activated chlorine with NO_2. This chlorine activation is likely to have happened during the short cold period at the beginning of December. With the beginning photolysis of HNO_3, the resulting NO_2 reacts rapidly with ClO to form $ClONO_2$ yielding a second maximum at about 20 km altitude. The SLIMCAT model clearly overestimates the amount of $ClONO_2$ in the whole altitude region whereas KASIMA underestimates $ClONO_2$ especially in the altitude region between 16 and 20 km. This could be explained by differences in the temperature fields used in the CTMs resulting in different amounts of chlorine activation especially in situations where the temperatures were close to the NAT threshold.

[29] Below 28 km the amount of N_2O_5 rapidly decreases with decreasing altitude due to the fact that the lower stratosphere is highly depleted in NO_x. SLIMCAT clearly underpredicts the amount of N_2O_5 in the stratosphere. This could be partly explained by the overestimation of the reaction $N_2O_5 + H_2O(s) \rightarrow 2\ HNO_3(s)$ owing to the overestimation of the aerosol loading in the model. The aerosol loading in the SLIMCAT model is higher compared to the SAGE II data by a factor of 4 at 17 km. This leads to an overestimation of HNO_3 which is indeed seen in the data in an altitude region below 18 km. In case of KASIMA there is a better agreement between the measured N_2O_5 values and the model results having in mind the inconsistency in the NO_y profile. Below about 22 km the amount of N_2O_5 is underestimated by KASIMA, too.

[30] HO_2NO_2 is a minor constituent which provides a link between the NO_x and HO_x compounds. The profile shows very low mixing ratios due to low amounts of NO_x and HO_x in the winter polar vortex with a peak mixing ratio of 60 pptv at 11.7 hPa. Whereas above the maximum the coincidence between the modeled HO_2NO_2 profiles is quite good, the profiles below this altitude differ significantly with both models which overestimate the amount of HO_2NO_2 by more than a factor of two.

[31] In contrast to former results, the winter 1999 NO_2 SLIMCAT model output is in line with the results of MIPAS-B. The KASIMA results even show an overestimation of NO_2 which is a very uncommon feature which might be caused by the underestimation of ClO. NO_2 is quite important because chlorine radicals are passivated rapidly by NO_x. The amount of NO_x controls, therefore, the efficiency of catalytic ClO_x cycles destroying ozone.

[32] Since the modeled total reactive nitrogen (NO_y) may be uncertain due to its dependence on the initialization and long timescale transport, and to separate to a first order dynamical from chemical effects, the ratios X/NO_y (X = HNO_3, $ClONO_2$, $2N_2O_5$, HO_2NO_2, NO_2) are shown in Figure 6.

[33] The ratio HNO_3/NO_y is reproduced by the two models quite well both in shape and value. The increasing

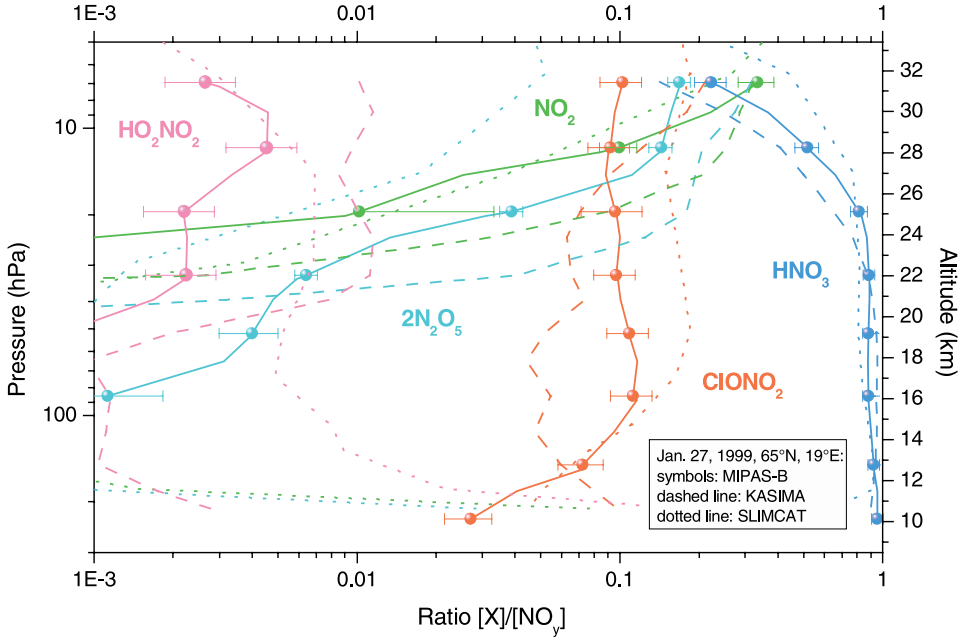

Figure 6. Comparison of the ratios of the individual NO_y components on 27 January 1999 (solid lines with symbols) compared to SLIMCAT (dotted lines) and KASIMA (dashed lines).

discrepancies with differences up to 40% between the two models above 25 km is owing to the different amounts of aerosol loading. The SLIMCAT model clearly overestimates the ratio $ClONO_2/NO_y$ above 16 km by up to 80% whereas KASIMA underestimates this ratio especially in the altitude region between 15 and 20 km by up to 60%.

[34] In contrast to former results the winter NO_2/NO_y SLIMCAT model output is in line with the results of MIPAS-B, while the KASIMA model results even show an overestimation. The ratio N_2O_5/NO_y is underestimated by SLIMCAT over the entire altitude region by a factor of 4. For KASIMA an overestimation by about 60% is found between 31 km and 22 km, but below 22 km the model also shows too low N_2O_5/NO_y ratios. These differences between the two models could be explained by the fact that KASIMA assumes a lower aerosol loading than SLIMCAT above about 13 km.

[35] The ratio HO_2NO_2/NO_y is overestimated by both models, which is a common feature, that is found in all comparisons between MIPAS-B results and model calculations [see, e.g., *Wetzel et al.*, 1997, 2002]. The overestimation of the HO_2NO_2/NO_y ratio in the models could possibly be explained by a new HO_2NO_2 photolysis pathway in the near infrared region not included in the models but postulated recently [*Salawitch et al.*, 2002]. The expected lower sunset values of HO_2NO_2 will result therefore in lower nighttime values.

6. Conclusions

[36] A characterization of the NO_y partitioning in the warm Arctic winter 1998/1999 was given. The MIPAS measurement on 27 January 1999 shows profiles of air masses with different character below and above 500 K clearly visible in the profiles of the long-lived trace gases N_2O and CH_4. Above 475 K the NO_y values are up to 2.5 ppbv lower than the reference correlation. This deficit can be attributed to mixing processes of subsided vortex air masses with extra-vortex air. The given mixing lines constructed with the help of the MIPAS CH_4–N_2O correlation can explain the deviations very well. Although temperatures were above the NAT thresholds for most of the time, the models, using currently recommended kinetic and photochemical parameters, fail to account for the observed partitioning within the NO_y family. Also, the agreement between the two CTMs KASIMA and SLIMCAT is not satisfactory. In particular, the description of the minor species HO_2NO_2 and N_2O_5 is not sufficient. The comparisons discussed above have clearly demonstrated that under such circumstances the understanding of the NO_y chemistry and our ability to model it is not satisfactory. It appears that part of this difficulty may be explained by the relatively warm, dynamically disturbed Arctic winter 1998/1999. During some periods of this winter stratospheric temperatures were close to the NAT threshold; in such a case the degree of chlorine activation is very sensitive to the model temperature. Another problem arises from the dynamic instability of the vortex which probably led to mixing processes on different scales which cannot be reproduced with coarsely resolved CTMs. Also other numerical problems like numerical mixing in the transport scheme in strong gradient regions should be taken into account. In any case, the synopsis of results from various geophysical situations indicates that the NO_y chemistry itself is not yet understood well, an issue which requires further attention in view of its importance for the fate of stratospheric ozone.

[37] **Acknowledgments.** The work presented in this paper was funded in part by the CEC Environmental Program (contract EV5V-CT93-0331) and the German Ozone Research Program (BMBF grant 01 LO 9401/9). We are grateful to the CNES launching team and the staff of the SSC Esrange for the excellent balloon operations and logistical support as well as ECMWF to provide us with meteorological data via NILU. We thank

B. Naujokat of FU Berlin for meteorological support and A. Engel for giving us the opportunity to compare our N_2O results to his data.

References

Bekki, S., and J. A. Pyle, A two-dimensional modeling study of the volcanic eruption of Mount Pinatubo, *J. Geophys. Res.*, *99*, 18,861–18,869, 1994.

Birk, M., and G. Wagner, A new spectroscopic database for chlorine nitrate, paper presented at Sixth Biennial HITRAN Database Conference 19–21 June 2000, Harvard-Smithsonian Cent. for Astrophys., Cambridge Mass., 2000.

Brasseur, G., and S. Solomon, Aeronomy of the middle atmosphere, in *Atmospheric Sciences Library*, pp. 275 and 283, D. Reidel, Norwell, Mass., 1986.

Brown, S. S., R. K. Talukdar, and A. R. Ravishankara, Reconsideration of the rate constants for the reaction $OH + NO_2 + M \rightarrow HNO_3 + M$ under atmospheric conditions, *Chem. Phys. Lett.*, *299*, 277–284, 1999a.

Brown, S. S., R. K. Talukdar, and A. R. Ravishankara, Reconsideration of the rate constants for the reaction of hydroxyl radicals with nitric acid vapor, *Chem. Phys. Lett.*, *103*, 3031–3037, 1999b.

Chipperfield, M. P., Multiannual simulations with a three-dimensional chemical transport model, *J. Geophys. Res.*, *104*, 1781–1805, 1999.

Clough, S. A., F. X. Kneizys, E. P. Shettle, and G. P. Anderson, Atmospheric radiance and transmittance: FASCOD2, paper presented at 6th Conference on Atmospheric Radiation, May 1986, Am. Meteorol. Soc., Boston, Mass., 1986.

Danilin, M. Y., et al., Nitrogen species in the post-Pinatubo stratosphere: Model analysis utilizing UARS measurements, *J. Geophys. Res.*, *104*, 8247–8262, 1999.

DeMore, W. B., et al., Chemical kinetics and photochemical data for use in stratospheric modeling, *JPL Publ. 94-26*, 1994.

DeMore, W. B., et al., Chemical kinetics and photochemical data for use in stratospheric modeling, *JPL Publ. 97-4*, 1997.

Dransfield, T. J., M. M. Sprengnether, K. K. Perkins, N. M. Donahue, J. G. Anderson, and K. L. Demerjian, Temperature and pressure dependent kinetics of the gas-phase reaction of the hydroxyl radical with nitrogen dioxide, *Geophys. Res. Lett.*, *26*, 687–690, 1999.

Fischer, H., and H. Oelhaf, Remote sensing of vertical profiles of atmospheric trace constituents with MIPAS limb-emission spectrometers, *Appl. Opt.*, *35*, 2787–2796, 1996.

Flaud, J.-M., Review of spectroscopic data for MIPAS, final report, *ESA Contract AOP/OL/RB/309204*, Eur. Space Res. and Technol. Cent., Noordwijk, Netherlands, 1992.

Friedl-Vallon, F., A. Kleinert, O. Trieschmann, H. Oelhaf, and G. Wetzel, Radiometric calibration of MIPAS-B2 spectra, paper presented at 8th International Workshop on Atmospheric Science from Space Using Fourier Transform Spectroscopy, Météo-France, Toulouse, France, 1998.

Friedl-Vallon, F., G. Maucher, H. Oelhaf, M. Seefeldner, O. Trieschmann, G. Wetzel, and H. Fischer, The balloon-borne Michelson Interferometer for Passive Atmospheric Sounding (MIPAS-B2)—Instrument and Results, in *Proc. SPIE Int. Soc. Opt. Eng., 3756*, 9–16, 1999.

Gao, R. S., et al., Partitioning of the reactive nitrogen reservoir in the lower stratosphere of the Southern Hemisphere: Observations and modeling, *J. Geophys. Res.*, *102*, 3935–3949, 1997.

Gao, R. S., et al., A comparison of observations and model simulations of NO_x/NO_y in the lower stratosphere, *Geophys. Res. Lett.*, *26*, 1153–1156, 1999.

Hofmann, D. J., and S. Solomon, Ozone destruction through heterogeneous chemistry following the eruption of El Chichon, *J. Geophys. Res.*, *94*, 5029–5041, 1989.

Jucks, K. W., D. G. Johnson, K. V. Chance, W. A. Traub, and R. J. Salawitch, Nitric acid in the middle stratosphere as a function of altitude and aerosol loading, *J. Geophys. Res.*, *104*, 26,715–26,723, 1999.

Kawa, S. R., Interpretation of NO_x/NO_y observations from AASE-II using a model of chemistry along the trajectories, *Geophys. Res. Lett.*, *20*, 2507–2510, 1993.

Kleinert, A., and F. Friedl-Vallon, Characterization of the non-linearity and the temperature dependence of the MIPAS-B2 detector system, paper presented at 8th International Workshop on Atmospheric Science from Space using Fourier Transform Spectroscopy, sponsor, Toulouse, France, 1998.

Kondo, Y., et al., NO_y–N_2O correlation observed inside the Arctic vortex in February 1997: Dynamical and chemical effects, *J. Geophys. Res.*, *104*, 8215–8224, 1999.

Kouker, W., I. Langbein, T. Reddmann, and R. Ruhnke, The Karlsruhe Simulation Model of the Middle Atmosphere (KASIMA), version 2, *Wiss. Ber. FZKA 7278*, 60 pp., Forschungs. Karlsruhe GmbH, Karlsruhe, Germany, 1999.

Lary, D. J., R. Toumi, A. M. Lee, M. J. Newchurch, M. Pirre, and J. B. Renard, Carbon aerosols and atmospheric photochemistry, *J. Geophys. Res.*, *102*, 3671–3682, 1997.

Lengel, A., F. Hase, M. Höpfner, and O. Trieschmann, Multi-line deconvolution of MIPAS-B2 high altitude spectra as a method to characterize its ILS, paper presented at 8th International Workshop on Atmospheric Science From Space Using Fourier Transform Spectroscopy, sponsor, Toulouse, France, 1998.

Manney, G. L., W. A. Lahoz, R. Swinbank, A. O'Neill, P. M. Connew, and R. W. Zurek, Simulation of the December 1998 stratospheric major warming, *Geophys. Res. Lett.*, *26*, 2733–2736, 1999.

Maucher, G., Das Sternreferenzsystem von MIPAS-B2: Sichtlinien-Bestimmung für ein ballongetragenes Spektrometer zur Fernerkundung atmosphärischer Spurengase, *Rep. FZKA 6227*, Forschungs. Karlsruhe GmbH, Karlsruhe, Germany, 1999.

Michelsen, H. A., G. L. Manney, M. R. Gunson, and R. Zander, Correlations of stratospheric abundances of NO_y, O_3, N_2O, and CH_4 derived from ATMOS measurements, *J. Geophys. Res.*, *103*, 28,347–28,359, 1998.

Michelsen, H. A., et al., Maintenance of high HCl/Cl_y and NO_x/NO_y in the Antarctic vortex: A chemical signature of confinement during spring, *J. Geophys. Res.*, *104*, 26,419–26,436, 1999.

Morris, G. A., et al., Nitrogen partitioning in the middle stratosphere as observed by UARS, *J. Geophys. Res.*, *102*, 8955–8965, 1997.

Müller, M., A. Engel, U. Schmidt, and F. Lefèvre, Structure of vertical profiles of long lived trace gases: A basis for the analysis of stratospheric dynamics, in *Stratospheric Ozone 1999: Proceedings of the 5th European Symposium 27 September to 1 October 1999*, edited by N. R. P. Harris, M. Guirlet, and G. T. Amanatidis, pp. 554–557, Eur. Comm., Brussels, 2000.

Nash, E., P. Newman, J. Rosenfield, and M. Schoeberl, An objective determination of the polar vortex using Ertel's potential vorticity, *J. Geophys. Res.*, *101*, 9471–9478, 1996.

Norton, H., and R. Beer, New apodization functions for Fourier spectroscopy, *J. Opt. Soc. Am.*, *66*, 259–264, 1976 (Errata J. Opt. Soc. Am., 67, 419, 1977).

Oelhaf, H., et al., Correlative balloon measurements of the vertical distribution of N_2O, NO, NO_3, HNO_3, N_2O_5, $ClONO_2$, and total reactive NO_y inside the polar vortex during SESAME, in *Polar Stratospheric Ozone: Proceedings of the 3rd European Workshop 18 to 22 September 1995*, edited by J. A. Pyle, N. R. P. Harris, and G. T. Amanatidis, pp. 187–192, Eur. Comm., Brussels, 1996.

Oelhaf, H., et al., Denitrification and mixing in the 1994/1995 arctic vortex derived from MIPAS-B measurements and modeling, *Stratospheric Ozone 1999: Proceedings of the 5th European Symposium 27 September to 1 October 1999*, edited by N. R. P. Harris, M. Guirlet, and G. T. Amanatidis, pp. 292–295, Eur. Comm., Brussels, 2000.

Oelhaf, H., et al., Inter-consistency checks of $ClONO_2$ retrievals from MIPAS-B spectra using different bands and spectroscopic parameter sources, in *IRS2000: Current Problems in Atmospheric Radiation: Proceedings International Radiation Symposium, St. Petersburg, Russia, 24–29 July 2000*, edited by W. L. Smith and Y. M. Timofeyev, pp. 615–618, A. Deepak, Hampton, Va., 2001.

Osterman, G. B., B. Sen, G. C. Toon, R. J. Salawitch, J. J. Margitan, and J.-F. Blavier, The partitioning of reactive nitrogen species in the summer Arctic stratosphere, *Geophys. Res. Lett.*, *26*, 1157–1160, 1999.

Payan, S., C. Camy-Peyret, P. Jeseck, T. Hawat, M. Pirre, J. B. Renard, C. Robert, F. Lefévre, H. Kanzawa, and Y. Sasano, Diurnal and nocturnal distribution of stratospheric NO_2 from solar and stellar occultation measurements in the Arctic vortex: Comparison with models and ILAS measurements, *J. Geophys. Res.*, *104*, 21,585–21,593, 1999.

Plumb, R. A., D. W. Waugh, and M. P. Chipperfield, The effects of mixing on tracer relationships in the polar vortices, *J. Geophys. Res.*, *105*, 10,047–10,062, 2000.

Portmann, R. W., S. S. Brown, T. Gierczak, R. K. Talukdar, J. B. Burkholder, and A. R. Ravishankara, Role of nitrogen oxides in the stratosphere: A reevaluation based on laboratory studies, *Geophys. Res. Lett.*, *26*, 2387–2390, 1999.

Randeniya, L. K., I. C. Plumb, and K. R. Ryan, NO_y and Cl_y partitioning in the middle stratosphere: A box model investigation using HALOE data, *J. Geophys. Res.*, *104*, 26,667–26,686, 1999.

Reddmann, T., R. Ruhnke, and W. Kouker, Three-dimensional model simulations of SF6 with mesospheric chemistry, *J. Geophys. Res.*, *106*, 14,525–14,537, 2001.

Rex, M., et al., Subsidence, mixing, and denitrification of Arctic polar vortex air measured during POLARIS, *J. Geophys. Res.*, *104*, 26,611–26,623, 1999.

Rothman, L. S., et al., The HITRAN Molecular Spectroscopic Database and HAWKS (HITRAN Atmospheric Workstation): 1996 Edition, *J. Quant. Spectrosc. Radiat. Transfer*, *60*, 665–710, 1998.

Salawitch, R. J., P. O. Wennberg, G. C. Toon, B. Sen, and J.-F. Blavier, Near IR photolysis of HO2NO2: Implications for HOx, *Geophys. Res. Lett.*, *29*(16), 1762, doi:10.1029/2002GL015006, 2002.

Sander, S. P., et al., Chemical kinetics and photochemical data for use in stratospheric modeling, *JPL Publ. 00-3*, 2000.

Sen, B., G. C. Toon, B. Osterman, J.-F. Blavier, J. J. Margitan, and R. J. Salawitch, Measurement of reactive nitrogen in the stratosphere, *J. Geophys. Res.*, *103*, 3571–3585, 1998.

Solomon, S., R. W. Portmann, R. R. Garcia, W. Randel, F. Wu, R. Nagatani, J. Gleason, L. Thomason, L. R. Poole, and M. P. McCormick, Ozone depletion at midlatitudes: Coupling of volcanic aerosols and temperature variability to anthropogenic chlorine, *Geophys. Res. Lett.*, *25*, 1871–1874, 1998.

Sugita, T., Y. Kondo, H. Nakajima, U. Schmidt, A. Engel, H. Oelhaf, G. Wetzel, M. Koike, and P. A. Newman, Denitrification observed inside the Arctic vortex in February 1995, *J. Geophys. Res.*, *103*, 16,221–16,234, 1998.

Thomason, L. W., L. R. Poole, and T. Deshler, A global climatology of stratospheric aerosol surface area density deduced from Stratospheric Aerosol and Gas Experiment II measurements: 1984–1994, *J. Geophys. Res.*, *102*, 8967–8976, 1997.

Trieschmann, O., Phasenkorrektur und Radiometrie gekühlter Fourierspektrometer: Charakterisierung des Instrumentes MIPAS-B2, *Rep. FZKA 6611*, Forschungs. Karlsruhe GmbH, Karlsruhe, Germany, 2000.

Trieschmann, O., and F. Friedl-Vallon, Parameterization of MIPAS-B2 non-linearity and calibration scheme, paper presented at 8th International Workshop on Atmospheric Science from Space Using Fourier Transform Spectroscopy, 16–18 Nov., xxxMétéo-France, Toulouse, France, 1998.

von Clarmann, T., RAT: A computational tool for the retrieval of atmospheric trace gas profiles from infrared spectra, *Rep. KfK 5423*, Forschungs. Karlsruhe GmbH, Karlsruhe, Germany, 1994.

von Clarmann, T., G. Wetzel, H. Oelhaf, F. Friedl-Vallon, A. Linden, G. Maucher, M. Seefeldner, O. Trieschmann, and F. Lefèvre, $ClONO_2$ vertical profile and estimated mixing ratios of ClO and HOCl in the winter Arctic stratosphere from Michelson interferometer for passive atmospheric sounding limb emission spectra, *J. Geophys. Res.*, *102*, 16,157–16,168, 1997.

von König, M., et al., Using gas-phase nitric acid as an indicator of PSC composition, *J. Geophys. Res.*, *107*, doi:10.1029/2001JD001041, in press, 2002.

Waibel, A. E., T. Peter, K. S. Carslaw, H. Oelhaf, G. Wetzel, P. J. Crutzen, U. Pöschl, A. Tsias, E. Reimer, and H. Fischer, Arctic ozone loss due to denitrification, *Science*, *283*, 2064–2068, 1999.

Waugh, D. W., et al., Mixing of polar vortex air into midlatitudes as revealed by tracer-tracer scatterplots, *J. Geophys. Res.*, *102*, 13,119–13,134, 1997.

Wennberg, E. L., et al., Removal of stratospheric O_3 by radicals: In situ measurements of OH, HO_2, NO, NO_2, ClO, and BrO, *Science*, *266*, 398–404, 1994.

Wetzel, G., T. von Clarmann, H. Oelhaf, and H. Fischer, Vertical profiles of N_2O_5 along with CH_4, N_2O, and H_2O in the late Arctic winter retrieved from MIPAS-B infrared limb emission measurements, *J. Geophys. Res.*, *100*, 23,173–23,181, 1995.

Wetzel, G., H. Oelhaf, T. von Clarmann, H. Fischer, F. Friedl-Vallon, G. Maucher, M. Seefeldner, O. Trieschmann, and F. Lefèvre, Vertical profiles of N_2O_5, HO_2NO_2, and NO_2 inside the Arctic vortex, retrieved from nocturnal MIPAS-B2 infrared limb emission measurements in February 1995, *J. Geophys. Res.*, *102*, 19,177–19,186, 1997.

Wetzel, G., et al., NO_y partitioning and budget and its correlation with N_2O in the Arctic vortex and in summer mid-latitudes in 1997, *J. Geophys. Res.*, *107*(D16), 4280, doi:10.1029/2001JD000916, 2002.

M. P. Chipperfield, School of the Environment, University of Leeds, Leeds, LS2 9JT, UK. (martyn@env.leeds.ac.uk)

H. Fischer, F. Friedl-Vallon, W. Kouker, G. Maucher, H. Oelhaf, T. Reddmann, R. Ruhnke, M. Stowasser, O. Trieschmann, T. von Clarmann, and G. Wetzel, Institut für Meteorologie und Klimaforschung, Forschungszentrum Karlsruhe, P.O.B. 3640, D-76021 Karlsruhe, Germany. (markus.stowasser@imk.fzk.de)